Natural Resources Canada | Ressources naturelles Canada

GEOMATICS CANADA
OPEN FILE 24

Evaluation of Multi-dimensional DInSAR for Permafrost Environments

N.H. Short

2016

Canada

GEOMATICS CANADA
OPEN FILE 24

Evaluation of Multi-dimensional DInSAR for Permafrost Environments

N.H. Short

2016

doi:10.4095/297626

This publication is available for free download through GEOSCAN (http://geoscan.nrcan.gc.ca/).

Recommended citation
Short, N.H., 2016. Evaluation of Multi-dimensional DInSAR for Permafrost Environments; Geomatics Canada, Open File 24, 21 p. doi:10.4095/297626

Publications in this series have not been edited; they are released as submitted by the author.

Executive Summary

Satellite interferometric radar (InSAR) is emerging as an excellent tool to monitor terrain stability. This report evaluates the newest techniques of two- and three-dimensional InSAR, applied specifically in permafrost terrain. Three-dimensional InSAR, as implemented here, is seen to be less reliable than two-dimensional InSAR. Two-dimensional InSAR provides valuable information about slope processes and the nature of terrain movement.

Résumé

Interférométrie radar par satellite (InSAR) est un excellent outil pour surveiller la stabilité du terrain. Ce rapport évalue les nouvelles techniques d'InSAR à deux et trois dimensions, appliquées spécifiquement dans le pergélisol. L'InSAR à trois dimensions, mis en œuvre ici, est considéré comme moins fiable que l'InSAR à deux dimensions. InSAR à deux dimensions fournit des informations précieuses sur les processus de pente et la nature du mouvement de terrain.

Table of Contents

List of Tables

List of Figures

1. Background

Differential Interferometric Synthetic Aperture Radar (DInSAR) delivers one-dimensional ground displacement information in the radar line-of-sight direction (LOS). While this is informative, it would be desirable to understand the full three-dimensional picture of ground displacement, to better identify mechanisms and causes of terrain instability. As DInSAR processing has matured, attempts have been made to overcome the LOS limitation by combining DInSAR data sets from different look directions, and/or combining DInSAR data with ancillary data sources. An excellent review of the various approaches in the literature, including a detailed summary table is provided by Hu et al. (2014).

While there are many approaches available, such as combining DInSAR with offset tracking, ancillary GPS data or multi-aperture InSAR data, these methods are either limited to large deformation signatures (> 10 cm), or rely on ancillary data. Deformation signatures in permafrost terrain are usually small (< 10 cm per summer season), and additional ancillary data is often simply not available in northern, remote permafrost regions. For small scale ground deformation without ancillary data, there are only two approaches that are currently possible: 1) multi-pass DInSAR at very high latitudes to extract three-dimensional displacement (Gray, 2011), or 2) simply neglecting the north-south displacement and combining ascending and descending geometries to extract two-dimensional displacement (Wright et al., 2004; Manzo et al., 2006).

In this report we examine the information content of simple two-dimensional DInSAR products using the equations of Manzo et al. (2006) and attempt to implement the three-dimensional solution of Gray (2011) in permafrost terrain.

2. Study sites and data sources

Three permafrost sites were used for the multi-dimensional DInSAR experiments, Herschel Island in the Yukon, and Slidre Fiord and Pangnirtung both in Nunavut. All sites lie within the continuous permafrost zone. Table 1 documents the site coordinates and the elevation and SAR data sources used in the DInSAR processing. We combined SAR data sets from a single sensor, RADARSAT-2, in our DInSAR processing.

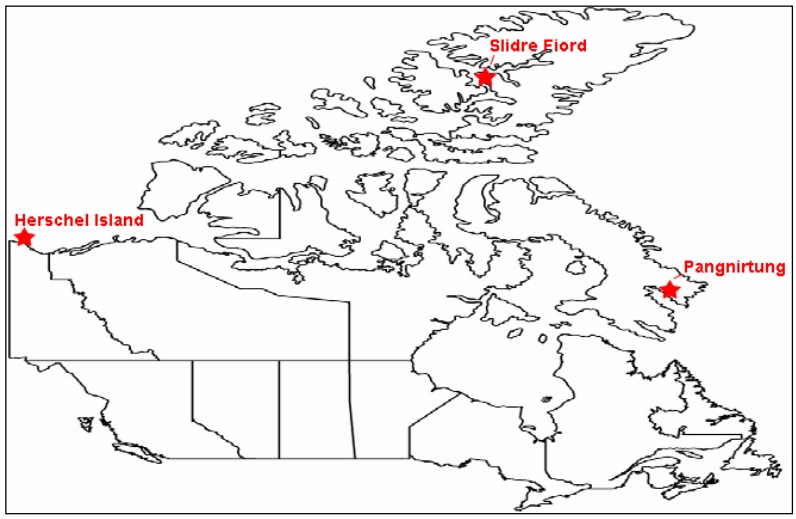

Figure 1. Outline map of Canada with provincial and territorial boundaries and the Herschel Island, Slidre Fiord and Pangnirtung study sites.

Table 1. Study sites and data

Study site (lat,long)	*Elevation data*	*RADARSAT-2 acquisitions* ***Mode-Path*** *(YYYYMMDD)*	*Look angle (°)*	*Incidence angle (°)*	*Azimuth angle (°) Clockwise from east*[1]
Herschel Island (69°35'N, 139°05'W)	2 m horizontal resolution from stereo IKONOS data	**U10-Asc** (20110908, 20120809)	34.66	39.79	256.60
		U11-Desc (20110902, 20120803)	33.62	38.60	102.73
Pangnirtung (66°09'N, 65°42'W)	1 m horizontal resolution from stereo Worldview-2 data	**SLA27-Asc** (20110612, 20110706, 20110730, 20110823, 20110919)	42.10	49.01	262.53
		SLA25-Desc (20110626, 20110720, 20110813, 20110906, 20110930)	41.10	47.84	97.59
Slidre Fiord (79°54'N, 85°54'W)	1 m horizontal resolution from stereo Worldview-1 data	**U1-Asc** (20130619, 20130806)	26.74	30.49	240.36
		U16-Asc (20120619, 20120713, 20120806, 20120830, 20120923, 20130614, 20130708, 20130801, 20140609, 20140703, 20140727, 20140820, 20140913)	36.52	42.14	250.84
		U2-Desc (20130713, 20130806, 20140614, 20140801, 20140825, 20140918)	27.49	31.33	118.04
		U24-Desc (20120616, 20140710, 20120803, 20120827, 20120920, 20130611, 20130705, 20130729, 20140630, 20140724, 20140910)	40.73	47.30	102.30

[1] Azimuth angle is given as clockwise from east, as required for the equations of Gray (2011). To convert to the more conventional clockwise from north, add 90 degrees.

3. Methods

The DInSAR processing was carried out using GAMMA software (Werner et al., 2000), and followed the conventional steps of image co-registration, interferogram formation, topographic phase removal using an external digital elevation model (DEM), baseline refinement, phase filtering (Goldstein and Werner, 1998) and phase unwrapping (Costantini, 1998). Further details on the method may be found in Short et al. (2014). For Herschel Island two interferometric pairs spanning September 2011 to August 2012 were used. For Pangnirtung two stacks of data spanning June to September 2011 were used. For Slidre Fiord, ascending and descending stacks from the summer of 2012 were used for the two-dimensional solution. For the three-dimensional solution multiple data sets spanning a 48 day summer period in 2013 and a three month summer period in 2014 were used. Stacking was used wherever possible to extract a linear rate of summer displacement and reduce noise in the results. Seasonal displacement of the active layer in permafrost terrain is typically small < 10 cm, therefore stacking aids in reducing noise and extracting the subtle trends (Lyons and Sandwell, 2003). All resulting phase rates were converted to displacement in centimetres in the radar line-of-sight (LOS).

3.1 Two-dimensional experiments

Line-of-sight displacements from ascending and descending paths were combined to calculate the east-west (d_e) and vertical (d_u - up-down) displacement components using the equations of Manzo et al. (2006). The original equations of Manzo et al. assume that the ascending and descending orbits are parallel and that the LOS directions are directly opposite, which is the case for Envisat and the ERS satellites near the Equator. There is however, a small deviation from this assumption because of the different beam modes available with RADARSAT-2 and the high latitudes of our sites. Our equations are a slight modification of the originals, to take into account the different beam modes of RADARSAT-2.

$$d_{east\_west} = \left(\frac{d_{LOS\_desc}}{\sin \gamma_{desc}} - \frac{d_{LOS\_asc}}{\sin \gamma_{asc}} \right) / 2$$

$$d_{vertical} = \left(\frac{d_{LOS\_desc}}{\cos \gamma_{desc}} + \frac{d_{LOS\_asc}}{\cos \gamma_{asc}} \right) / 2$$

Where:

d_{LOS} is the displacement in the line-of-sight of the data set.

γ is the look angle of the data set

The look angle is not provided automatically with the RADARSAT-2 product and must be calculated from the SAR scene ancillary data, this calculation was implemented using an in-house Perl script. Since the look angle remains constant for each beam mode of RADARSAT-2 it would be possible to automate this step in the future. The two-dimensional equations given above were implemented using GAMMA programs and an in-house Perl script.

3.2 Three-dimensional experiments

The equations of Gray (2011) were only implemented at our highest latitude site – Slidre Fiord (79°54'N). The equations were implemented using GAMMA programs and an in-house Perl script. The derivation of d_e, d_n and d_u is based on the matrix given in the accompanying material of Gray (2011):

$$\begin{bmatrix} d_e \\ d_n \\ d_u \end{bmatrix} = \left(\begin{bmatrix} A & D & G \\ B & E & H \\ C & F & K \end{bmatrix} \begin{bmatrix} \delta_a \\ \delta_b \\ \delta_c \end{bmatrix} \right) / \det(T)$$

Where:

$d_{e,n,u}$ are the displacements in the east, north and up directions
$\delta_{a,b,c}$ are the LOS displacements for passes a, b and c.
A through K are defined as:

$$A = \sin\chi_b \sin\theta_b \cos\theta_c - \cos\theta_b \sin\chi_c \sin\theta_c$$
$$B = -\cos\theta_b \cos\chi_c \sin\theta_c + \cos\chi_b \sin\theta_b \cos\theta_c$$
$$C = \sin\theta_b \sin\theta_c \sin(\chi_b - \chi_c)$$
$$D = \cos\theta_a \sin\chi_c \sin\theta_c - \sin\chi_a \sin\theta_a \cos\theta_c$$
$$E = -\cos\chi_a \sin\theta_a \cos\theta_c + \cos\theta_a \cos\chi_c \sin\theta_c$$
$$F = \sin\theta_a \sin\theta_c \sin(\chi_c - \chi_a)$$
$$G = \sin\chi_a \sin\theta_a \cos\theta_b - \cos\theta_a \sin\chi_b \sin\theta_b$$
$$H = -\cos\theta_a \cos\chi_b \sin\theta_b + \cos\chi_a \sin\theta_a \cos\theta_b$$
$$K = \sin\theta_a \sin\theta_b \sin(\chi_a - \chi_b)$$

where:

$\theta_{a,b,c}$ is the incidence angle of the pass (angle between the radar look vector and local vertical)
$\chi_{a,b,c}$ is the azimuth angle of the pass (clockwise from east, following Gray (2011))

and,

$$\det(T) = \sin\theta_a \sin\theta_b \sin\theta_c \left[\frac{\sin(\chi_a - \chi_c)}{\tan\theta_b} + \frac{\sin(\chi_c - \chi_b)}{\tan\theta_a} + \frac{\sin(\chi_b - \chi_a)}{\tan\theta_c} \right]$$

$\det(T)$ is the determinant of the matrix and is particularly important as it provides a measure of the strength of the matrix and therefore the reliability of the results. Values 0.2 to 1 are desirable, values < 0.2 will probably not yield reliable results.

The second part of the $\det(T)$ equation can be termed T1 and used to simplify the calculation of d_u:

$$T_1 = \left[\frac{\sin(\chi_a - \chi_c)}{\tan\theta_b} + \frac{\sin(\chi_c - \chi_b)}{\tan\theta_a} + \frac{\sin(\chi_b - \chi_a)}{\tan\theta_c} \right]$$

$$d_u = \frac{\sin(\chi_c - \chi_a)}{T_1 \sin\theta_b}\delta_b + \frac{\sin(\chi_a - \chi_b)}{T_1 \sin\theta_c}\delta_c + \frac{\sin(\chi_b - \chi_c)}{T_1 \sin\theta_a}\delta_a$$

The east-west and north-south components are derived from:

$$d_e = (A\delta_a + D\delta_b + G\delta_c)/\det(T)$$

$$d_n = (B\delta_a + E\delta_b + H\delta_c)/\det(T)$$

3.3 Dimensional limitations

Although theoretically multiple dimensions can be derived from DInSAR, it should be noted that the dimensions are not of equal quality. The accuracy of DInSAR measurements varies with dimension, due to the fixed paths and look directions of the satellites. The east-west and vertical dimensions are the best resolved, with precision on the order of mm (Wright et al., 2004). The north-south dimension is more difficult to resolve because earth observation satellites typically fly on a north-south path, and never directly measure displacement in this direction. Only at high latitudes do satellite orbits diverge sufficently from the north-south track to begin to capture some north-south displacement. Even then the sensitivity of the north-south component is significantly less than other directions and the precision of this component will be reduced by an order of magnitude (cm) (Wright et al., 2004).

4. Results

4.1. Herschel Island

The two-dimensional solution was applied to Herschel Island using a one year inter-annual data set. Figure 2 shows the LOS displacements calculated for ascending and descending DInSAR pairs spanning September 2011 to August 2012. Figure 3 shows the east-west and vertical displacements derived from the LOS data.

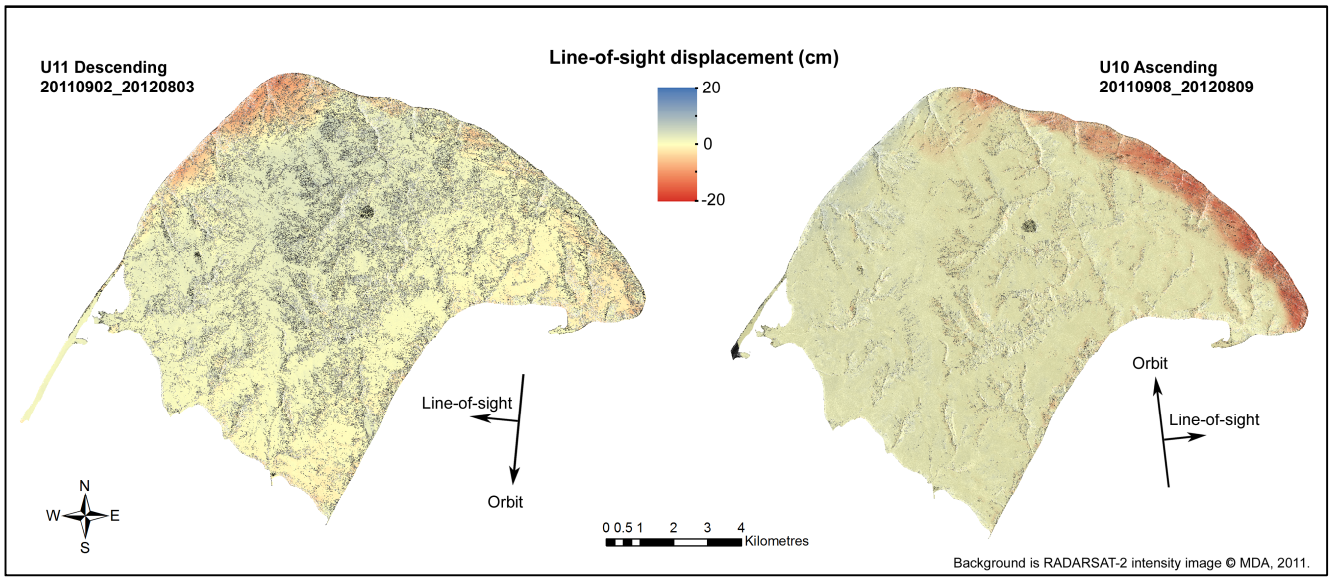

Figure 2. Herschel Island LOS displacements calculated for ascending and descending DInSAR pairs spanning September 2011 to August 2012. Negative values indicate movement away from the sensor.

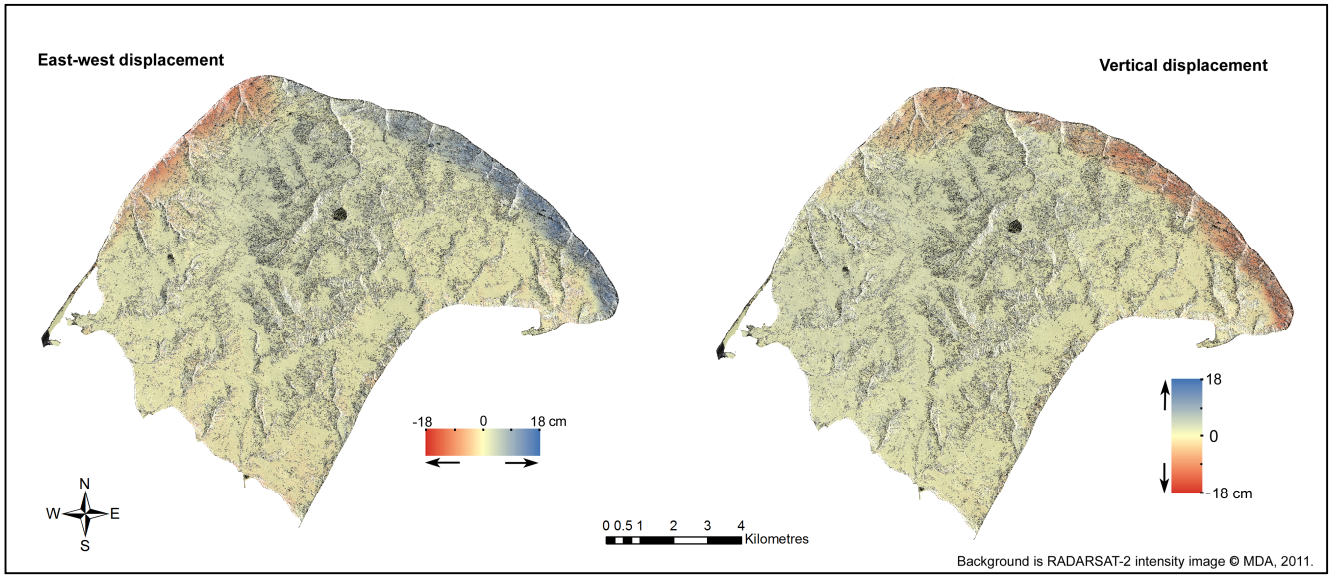

Figure 3. Herschel Island east-west and vertical displacements derived from DInSAR LOS data from September 2011 to August 2012.

While the coastline instability is visible in both the ascending and descending LOS data, the two-dimensional solution reveals the direction of the movement. The east-west component brings out the dramatic side slip that is happening along both the north-west and north-east coastlines and the vertical component brings out that downward motion is dominant along the north-east coastline and at the northern tip of the island, but is less significant on the north-west coastline. Figure 4 is the digital elevation model of the island and the steeper slopes along the northern coastlines can be seen, validating the likelihood of high horizontal and vertical displacements at these locations.

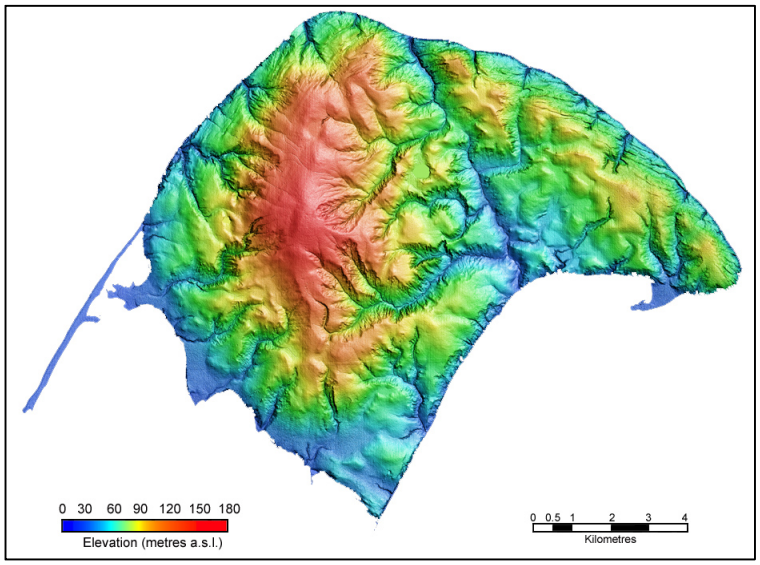

Figure 4. Digital elevation model of Herschel Island, derived from stereo-optical IKONOS imagery of 18 September, 2004. 2 m horizontal resolution.

4.2. Pangnirtung

Figure 5 shows the two-dimensional results for the community of Pangnirtung. The figure shows that the majority of the seasonal displacement in the Pangnirtung area is vertical downward, < 10 cm over 3 months. The east-west component is much less. This pattern of movement would be expected with summer thaw and settlement of the active layer.

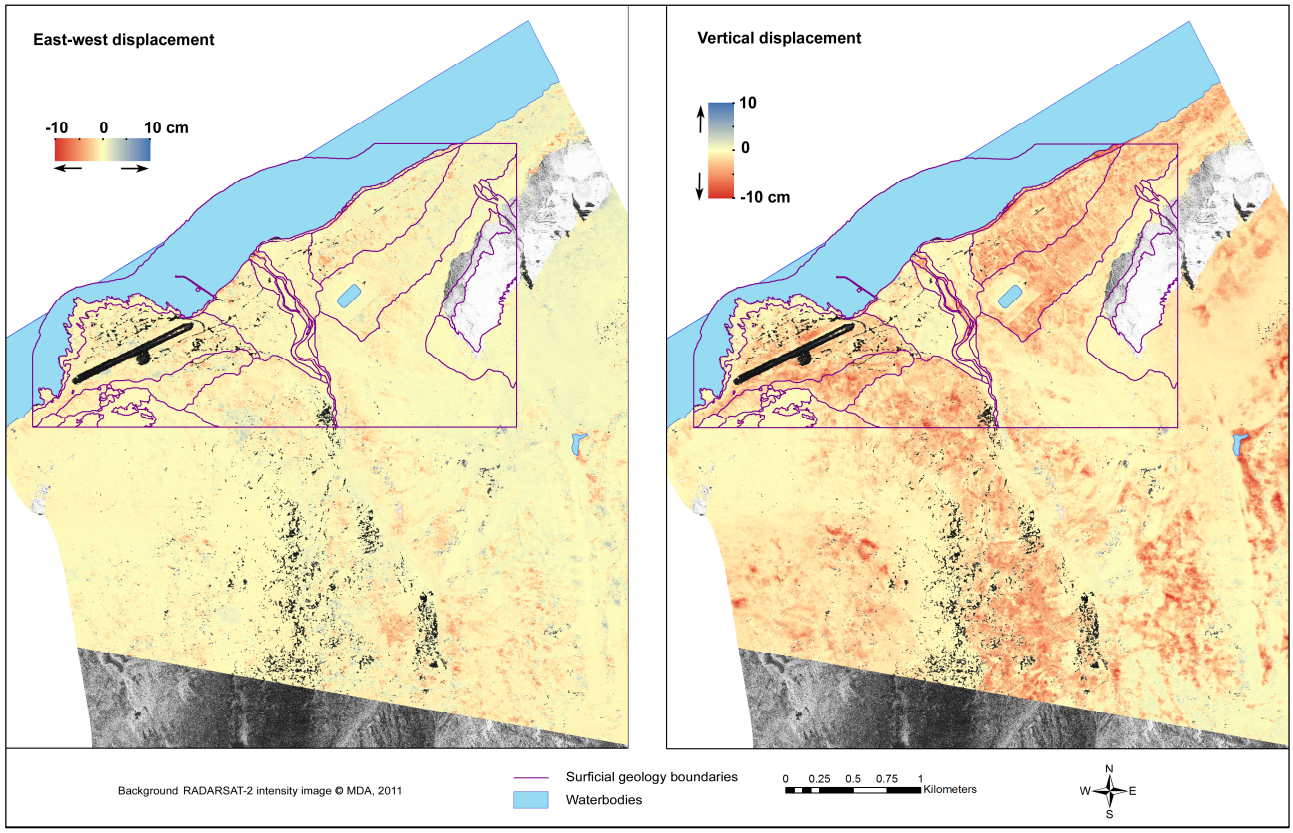

Figure 5. East-west and vertical displacement at Pangnirtung derived from ascending SLA27 and descending SLA25 RADARSAT-2 summer 2011 data stacks.

Figure 6 is the digital elevation map of the Pangnirtung area. While there are some steep slopes behind the community, the community itself, identifiable by the airport runway and the water reservoir, is located on relatively flat terrain along the edge of the fiord. It is therefore expected that displacements within the community should be predominately vertical.

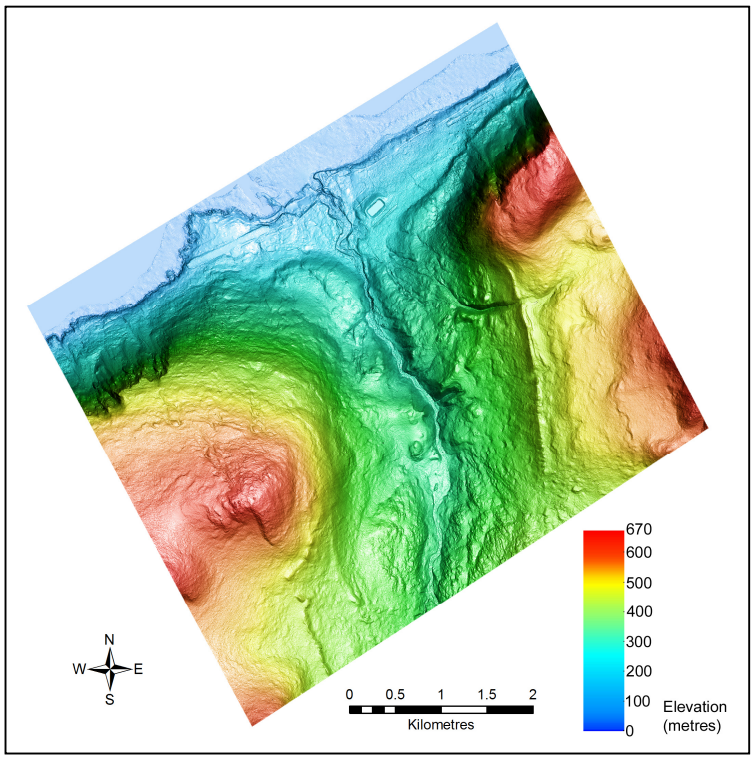

Figure 6. Digital elevation model of Pangnirtung and surrounding area, derived from stereo-optical Worldview-2 imagery of 10 July, 2010. 1 m horizontal resolution.

Figure 7 is a close up of the displacements around the airport runway and demonstrates interesting patterns in two specific locations (magenta circles). In general the area shows only vertical downward displacement, which would be expected for an active layer in generally flat terrain, however, at these two highlighted locations the vertical component becomes negligible and eastward displacement is seen on the order of 2 – 6 cm. Given the flat terrain, horizontal displacement would not be expected at these locations.

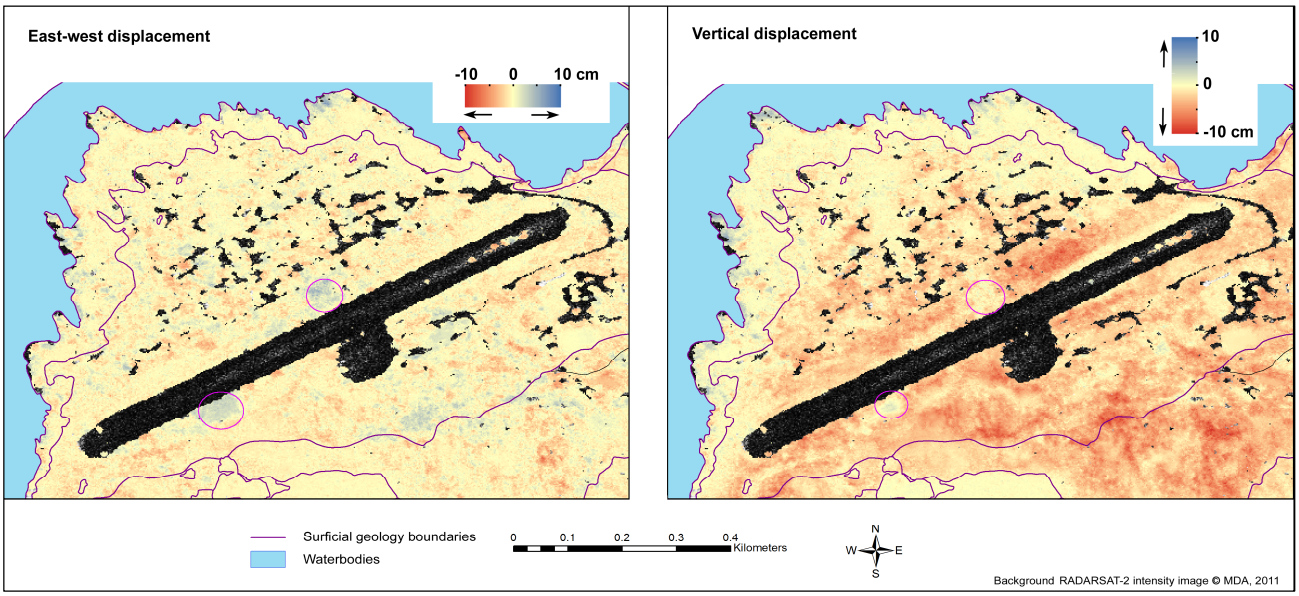

Figure 7. Detailed east-west and vertical displacement for the Pangnirtung Airport derived from 2011 DInSAR. Magenta circles identify two pockets of horizontal displacement discussed in the text.

The DEM, historical airphotos (last 50 years) and recent general field photos (last 5 years) do not reveal slopes or anything unique at these locations that would logically cause horizontal displacement. The calculated horizontal component is only the difference between the ascending and descending LOS contributions, therefore this could potentially just be a difference in the local conditions between the times of the ascending and descending acquisitions. The pockets of movement are considered unlikely to be atmospheric noise, since they are so small, and the process of stacking should eliminate or at least reduce randomly varying signatures. One last consideration is the possibility of the presence of clay sediments. Clay sediments are known to swell when wet and cause uplift of the ground surface which can be detected with DInSAR methods (Gabriel, Goldstein and Zebker, 1989). Different surface moisture conditions and thus different amounts of clay swelling and uplift at the times of the ascending and descending passes might therefore produce erroneous horizontal displacements. Borehole data in the general area from 1980 (Smith and Dallimore) show that bedrock is relatively shallow in this area between 1.6 and 6 m, covered by frozen silty sand. They documented clay content at less than 5%, suggesting that the potential for a DInSAR signal caused by clay swelling is low. A specific field visit to these locations would be needed to confirm ground conditions and identify potential causes of the displacement patterns.

4.3. Slidre Fiord

For Slidre Fiord two data stacks for summer 2012 (ascending U16 and descending U24) were used to derive the two-dimensional solution. Figure 8 shows the initial LOS displacements for those stacks and Figure 9 shows the two-dimensional result.

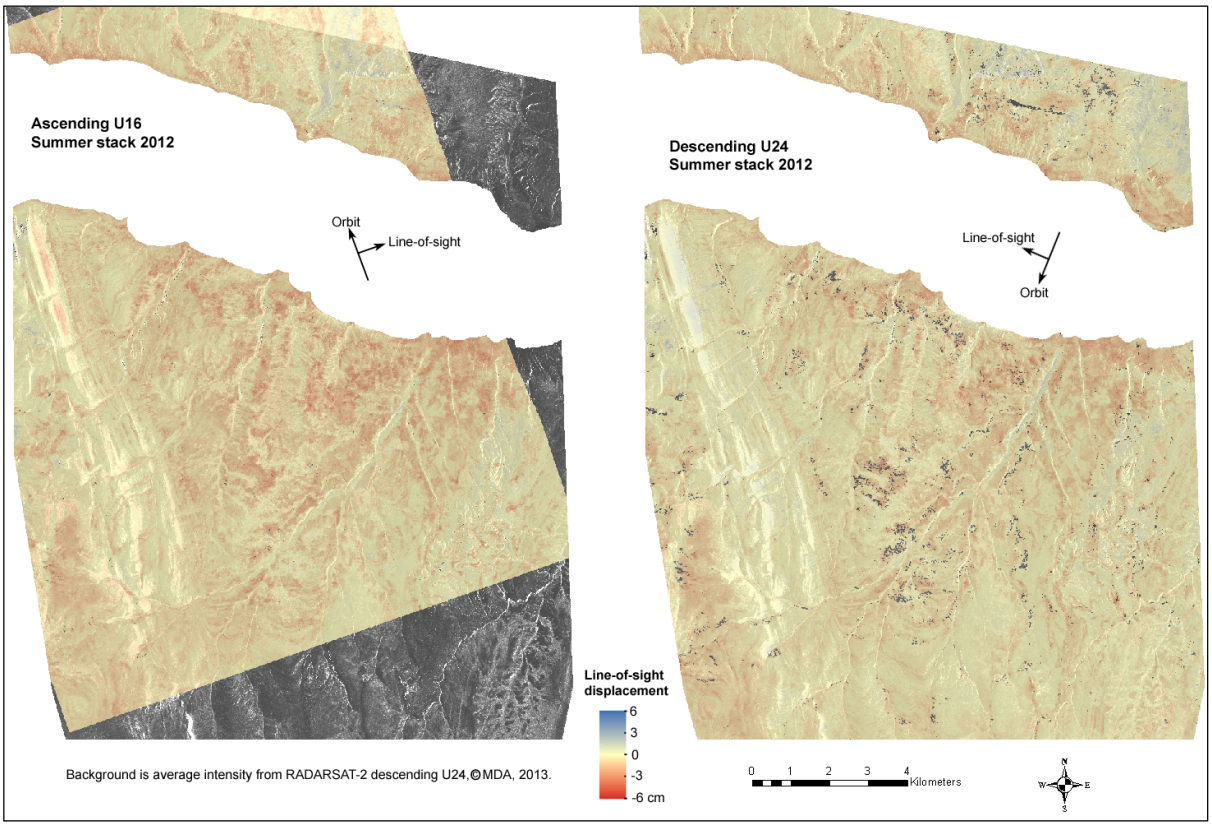

Figure 8. Slidre Fiord LOS displacements from ascending and descending DInSAR data stacks from June to August, 2012. Negative values indicate movement away from the sensor.

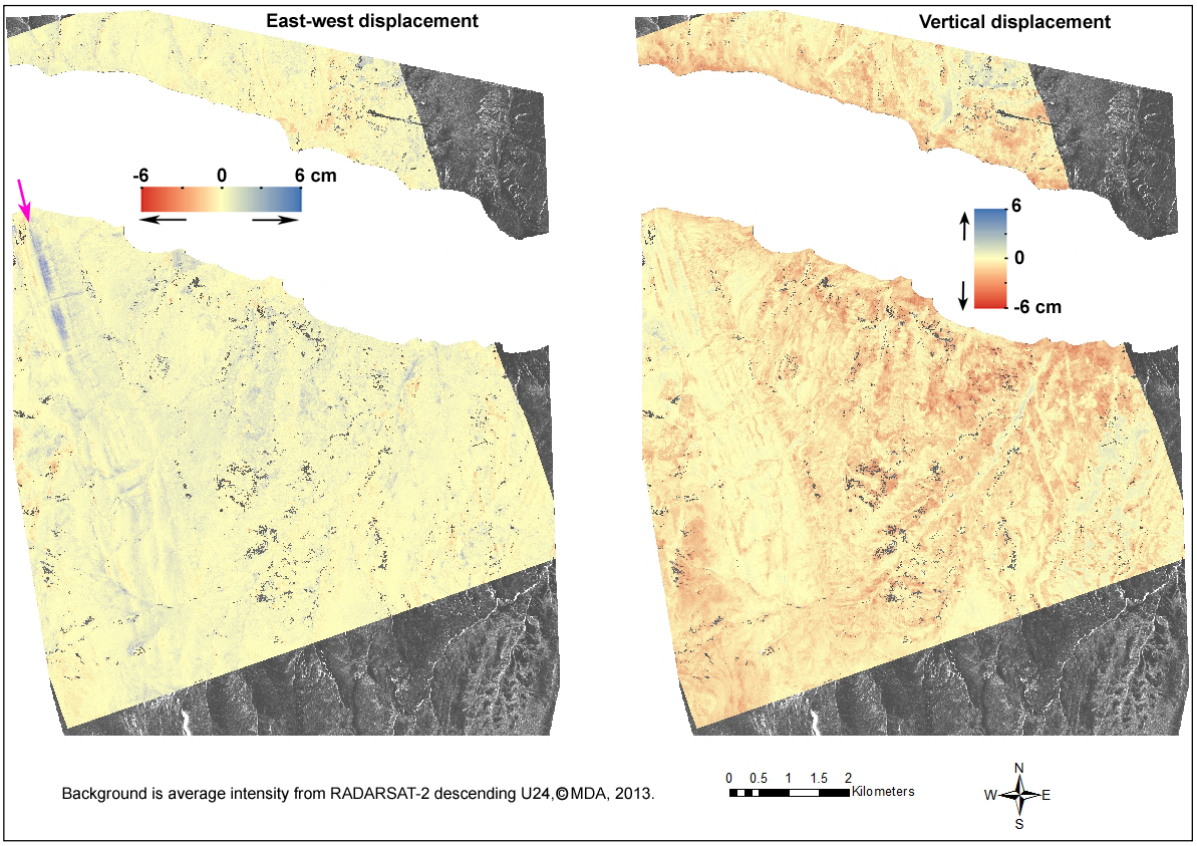

Figure 9. East-west and vertical displacements at Slidre Fiord derived from DInSAR data over the period June to August 2012. Magenta arrow indicates location of ridge and slope processes discussed in text.

Like Pangnirtung, the Slidre area also shows predominately vertical downward movement of the ground during the summer, which is consistent with the well understood seasonal settlement of the active layer in relatively flat terrain. Eastward displacement is well detected on the east facing slope of the ridge along the west side of the image (magenta arrow), indicative of slope processes. Some coherence loss is apparent at the bottom of this slope, suggesting surface disturbance due to accumulating material. Other subtle patches of horizontal motion are visible within the data coverage, likely related to slopes around stream channels.

Figure 10 shows the elevation data for Slidre Fiord. The generally low-lying terrain can be seen with the 600 m ridge feature on the west side, supporting the likelihood of slope processes noted in the east-west displacements.

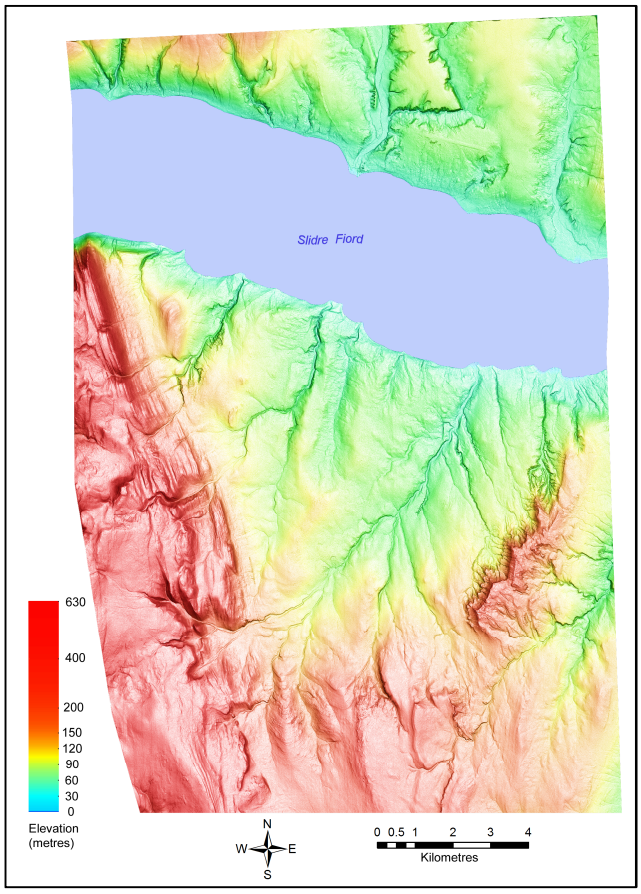

Figure 10. Terrain elevation in the Slidre Fiord area, derived from stereo-optical Worldview-1 data acquired 10 August, 2009. 1 m horizontal resolution.

4.4 Three-dimensional experiments at Slidre Fiord

Four RADARSAT-2 swaths were available over the Slidre site in 2013 and three in 2014: U24-Desc, U16-Asc, U2-Desc and U1-Asc (2013 only). Three passes were used in each Slidre processing, in an attempt to maximise the difference between the azimuth and incidence angles. Due to an unusually high amount of rain and snow in August 2013 only data from the early part of that summer were useful for interferometry. The data sets from 2013 only represent 48 days of ground displacement whereas the 2014 data cover three months.

The three-dimensional equations of Gray (2011) form a matrix. The determinant of the matrix determines the strength (reliability) of the three-dimensional solution. Determinant values of 0.2 – 1 are desirable for a reliable solution, i.e. the passes demonstrate sufficient variation in the azimuth angles to reliably separate the different displacement directions.

Scene centre determinants for the Slidre combination options were:

Combination 1 = U24-Desc, U16-Asc, U1-Asc Determinant: 0.0148
Combination 2 = U24-Desc, U16-Asc, U2-Desc Determinant: 0.0358
Combination 3 = U16-Asc, U1-Asc, U2-Desc Determinant: 0.0054
Combination 4 = U24-Desc, U1-Asc, U2-Desc Determinant: 0.0294

These are all much lower than the desired value of 0.2, indicating that the solutions might not be reliable.

While it is possible to process the data and extract results from the equations, the products are questionable. Figure 11 shows the 2013 products from the combination 2 processing (U24-D, U16-A, U2-D), the pass combination with the highest determinant.

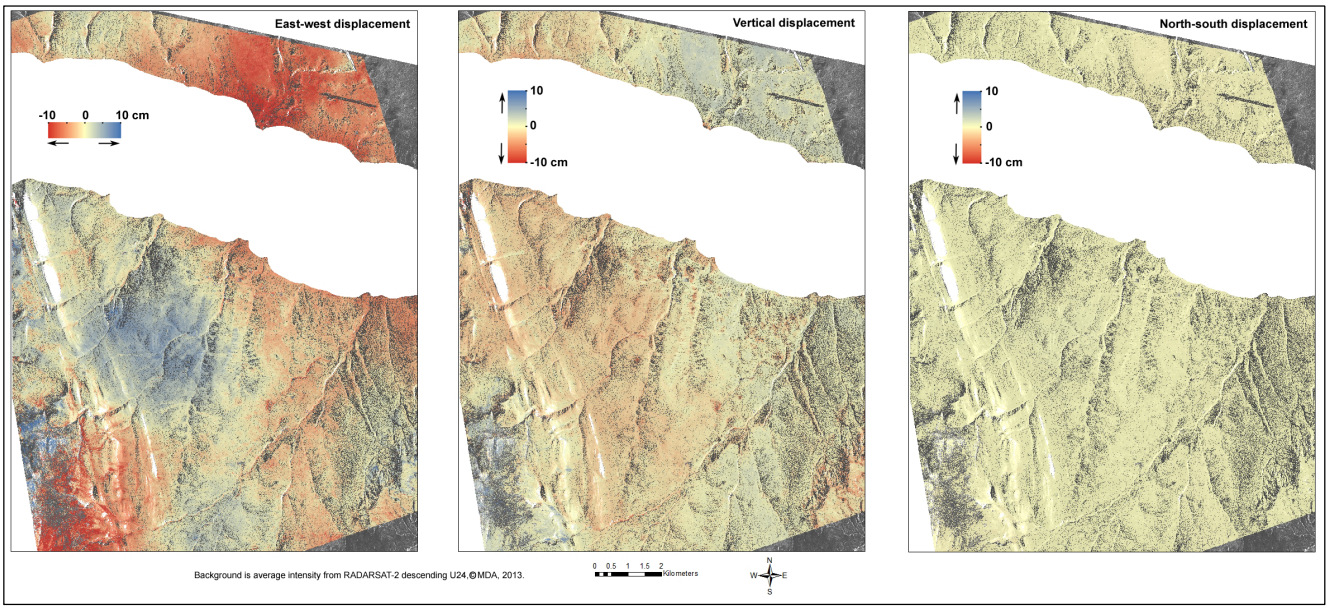

Figure 11. Three-dimensional result from Slidre Fiord 2013, using U24-D, U16-A and U2-D data sets as input.

The east-west component shows very large movement +/- 15 cm, which is unrealistic during the course of the summer. The vertical component (du) is also highly variable, +/- 10 cm, although this is a reasonable range the patterns are not aligned with geomorphology, therefore highly suspect. The extreme values in this data set could be a combination of unstable equations and atmospheric noise, since any atmospheric bias will be magnified in the three-dimensional solution.

Combination 1 (U24-D, U16-A, U1-A) was also processed, replacing the U2-D data with U1-A. While this data set had the lowest determinant, it was considered the least contaminated by atmospheric noise. The results in Figure 12 show that the displacement values are more realistic, however the patterns are still not well aligned with geomorphological features (especially noticeable in the east-west component). Therefore the values are still unlikely to be reliable. Neither data set shows the same patterns as shown in the 2012 two-dimensional solution.

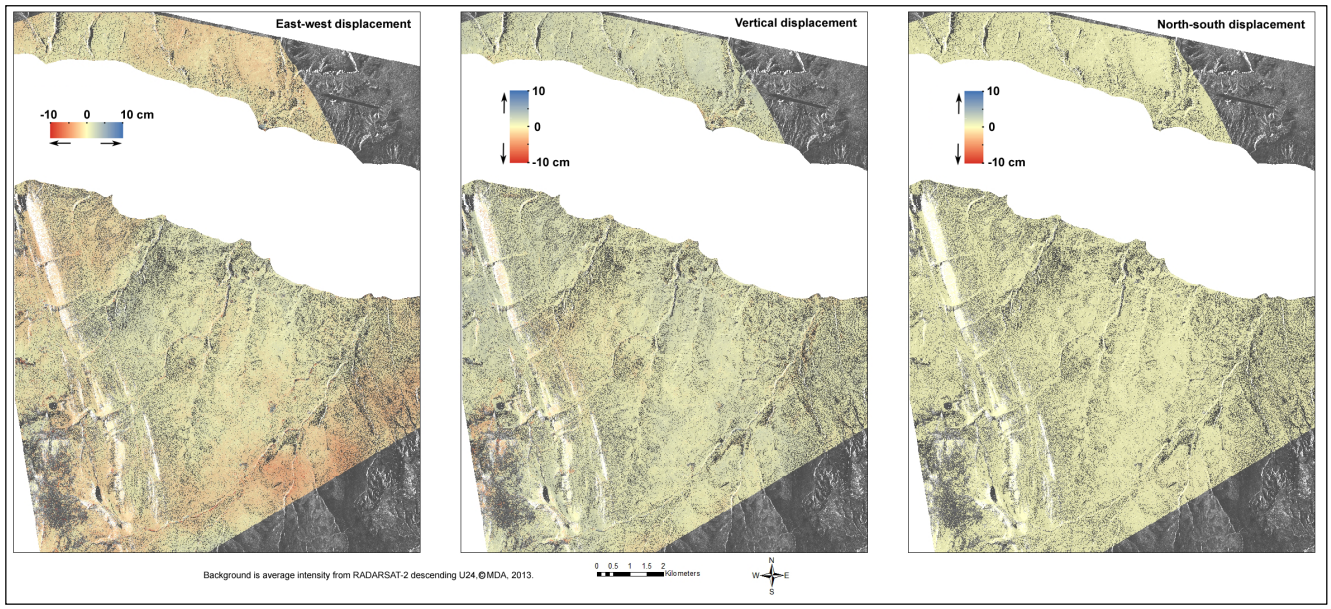

Figure 12. Three-dimensional result from Slidre Fiord 2013, using U24-D, U16-A and U1-D data sets as input.

The U24-D, U16-A, U2-D combination was also processed for 2014, this was a more complete data set with a longer observation period and large displacements of the ground detected in the LOS data. While the displacement patterns are aligned with geomorphology and therefore more likely to reflect geophysical processes, the displacement values are vastly larger than expected.

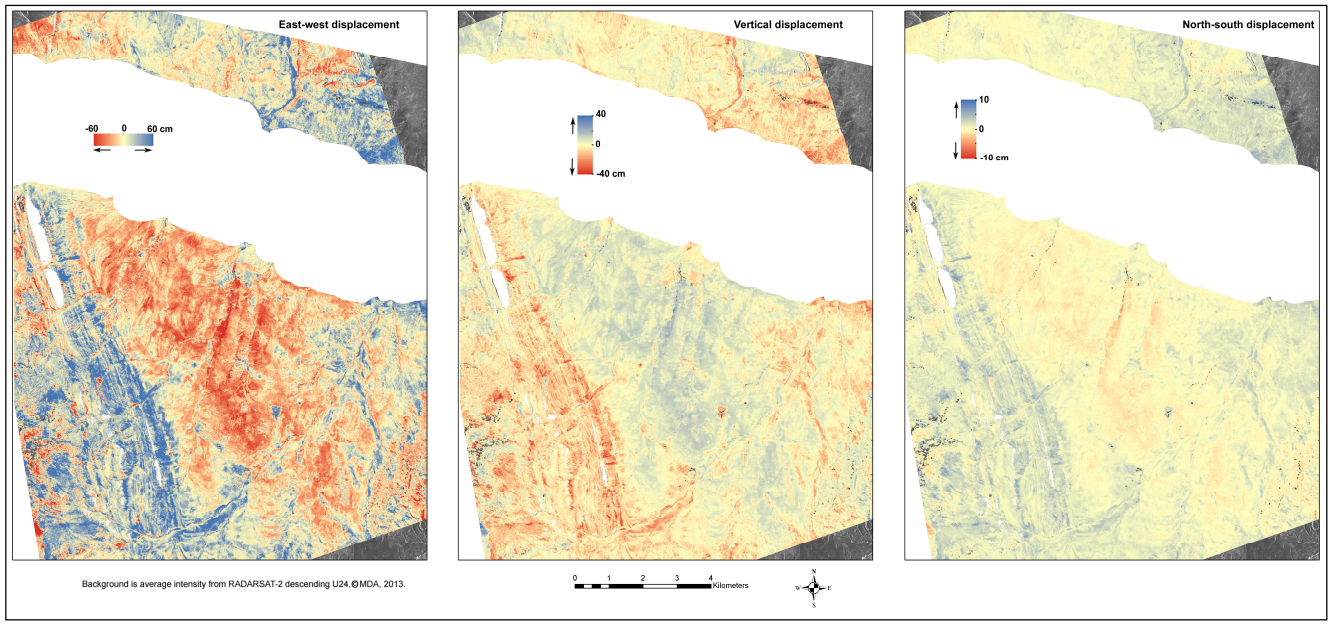

Figure 13. Three-dimensional result from Slidre Fiord 2014, using U24-D, U16-A and U2-D data sets as input. Note the different and large range of colour scales.

The 2014 U-16A and U24-D data processed to simple two-dimensional solution (Figure 14) showed patterns similar to those shown in Figure 9, although noticeably noisier, indicating that the 2014 data are a more challenging test for the three-dimensional equations. However, the fact that the two-dimensional solution still produces values in the expected range and identifies common trends over some geomorphological features indicates that the 2014 data are acceptable and that it is the results of the three-dimensional solution that are questionable.

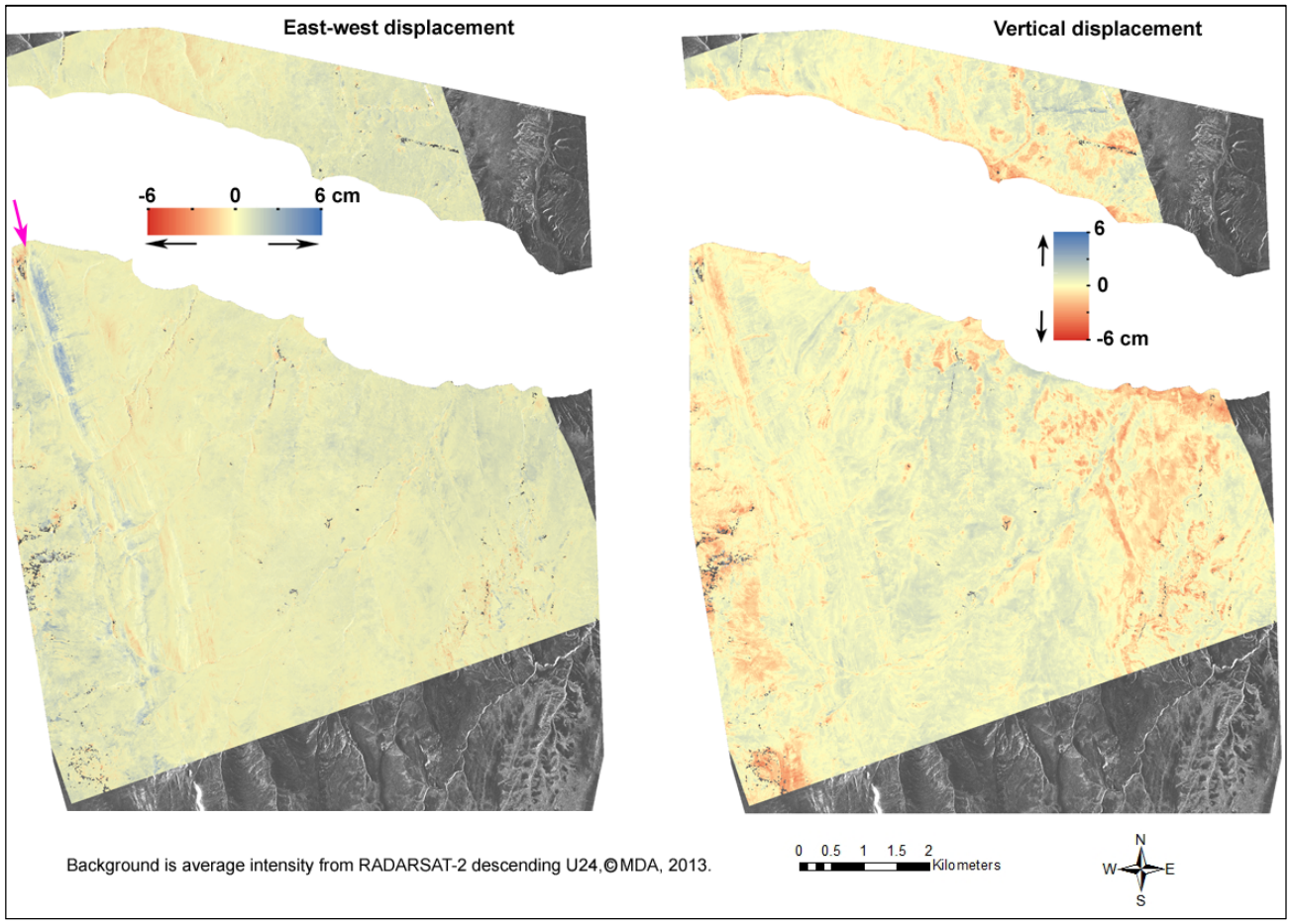

Figure 14. East-west and vertical displacements derived from U16-A and U24-D data over summer 2014. Ridge feature identified with magenta arrow.

It seems likely that differences between the ascending and descending acquisitions, possibly atmospheric related judging by the large scale of the patterns, have been magnified by the three-dimensional equations and resulted in questionable values in the three-dimensional products.

To check that the bizarre three-dimensional results were not the result of a scripting or implementation error, a test was performed using the original glaciology data of Gray (2011). Gray's patterns of vertical and horizontal glacier movement were well reproduced and of comparable magnitude, indicating that the disappointing Slidre results were indeed a consequence of low displacement values and unstable equations.

5. Conclusions

Although it is theoretically possible to perform three-dimensional DInSAR at high latitudes, even at close to 80°N the orbit crossings are not ideal to produce equations that are stable for small amounts of displacement. This application might be more successful further north, which of course vastly limits the region over which it could be applied. In addition, the displacements would need to be larger than is typically seen in permafrost terrain over a single season. Larger displacements would help to increase the signal above the noise and make for more reliable results. It is worth noting that the success of Gray (2011) was using glacier displacements of many metres horizontally and ~20 cm vertically, and at a latitude of 81°50'N.

While these three-dimensional results with RADARSAT-2 were not considered successful, it is possible that with opposing look directions (i.e. left- and right-looking satellites), or by combining observations from different satellites with more diversity in azimuth angles, these results could be improved upon.

In contrast, the two-dimensional method was simple to implement and produced intelligent results. These results identified slope processes versus purely vertical motion and offered insight into the geomorphological processes acting at a site. This was evident in the coastline processes on Herschel Island, the slope processes at Slidre Fiord and hinted at in the airport example from Pangnirtung. Combining two look directions also reduces the risk of missing significant motion at site, although the north-south displacements would still be unknown. The difficulty with this application can be acquiring both ascending and descending interferometric observations where there is competition for SAR time on the spacecraft. It may be worth the investment of effort if the site is a high risk site and infrastructure investments warrant a full and ongoing understanding of terrain instability.

6. Acknowledgements

This work was completed as part of the Remote Sensing Science Program at Natural Resources Canada. Much help was received from A.L. Gray for which the author is very grateful. Assistance with the Pangnirtung interpretation was provided by A-M. LeBlanc of the Geological Survey of Canada. This report also benefited from internal review and advice from S. Samsonov. The RADARSAT-2 data are copyright MacDonald, Dettwiler and Associates, and were provided by the Canadian Space Agency under the Canadian Government Data Allocation.

7. References

Costantini, M. (1998). A novel phase unwrapping method based on network programming. *IEEE Transactions on Geoscience and Remote Sensing*, 36(3), 813-821, doi:10.1109/36.673674.

Gabriel, A.K., Goldstein R.M., and Zebker, H.A. (1989). Mapping small elevation changes over large areas: Differential Radar Interferometry. *Journal of Geophysical Research*, 94(B7): 9183-9191.

Goldstein, R.M. & Werner, C.L. (1998). Radar interferogram filtering for geophysical applications. *Geophysical Research Letters*, 25(21), 4035–4038.

Gray, L. (2011). Using multiple RADARSAT InSAR pairs to estimate a full three dimensional solution for glacial ice movement. *Geophysical Research Letters*, 38(L05502). doi:10.1029/2010GL046484.

Hu J., Li, Z.W., Ding, X.L., Zhang, L and Sun, Q. (2014). Resolving three-dimensional surface displacements from InSAR measurements: A review. *Earth-Science Reviews*, 133: 1-17.

Lyons, S. and Sandwell, D. (2003). Fault creep along the southern San Andreas from interferometric synthetic aperture radar, permanent scatterers, and stacking. *Journal of Geophysical Research*, 108(B1), 2047, doi:10.1029/2002JB001831.

Manzo, M., Ricciardi, G.P., Casu, F, Ventura, G., Zeni, G., Borgström, S., Berardino, P., Del Gaudio, C. and Lanari, R. (2006). Surface deformation analysis in the Ischia Island (Italy) based on spaceborne radar interferometry. *Journal of Volcanology and Geothermal Research*, 151:399-416.

Short, N., LeBlanc, A.-M., Sladen, W., Oldenborger, G., Mathon-Dufour, V. and Brisco, B. (2014). RADARSAT-2 D-InSAR for ground displacement in permafrost terrain, validation from Iqaluit Airport, Baffin Island, Canada. *Remote Sensing of Environment*. 141:40-51. doi:10.1016/j.rse.2013.10.016

Smith, L. B. and Dallimore, S. R. (1980). Pangnirtung Land Assembly Geotechnical Investigation, File 15-22-9, submitted to Department of Public Works. Thurber Consultants Ltd, Edmonton, Alberta.

Werner, C., Wegmüller, U., Strozzi, T. and Wiesmann, A. (2000). GAMMA SAR and interferometric processing software. *Proceedings of ERS-Envisat Symposium*, Gothenburg, 16-20 October, 2000

Wright, T.J., Parsons, B.E. and Lu, Z. (2004). Toward mapping surface deformation in three dimensions using InSAR. Geophysical Research Letters, 31: L01607 http://dx.doi.org/10.1029/2003GL018827.